Modern Physics Letters B, Vol. 18, Nos. 12 & 13 (2004) 597–602

World Scientific
www.worldscientific.com

A CRYSTAL STRUCTURE STUDY OF $La_{1-x}Ca_xMnO_3$ NANOPARTICLES

YINGWEN DUAN* and JIANGONG LI

Institute of Materials Science and Engineering,
Lanzhou University, Lanzhou 730000, P. R. China
**duanyw@lzu.edu.cn*

Received 9 December 2003

Using a sol-gel method, $La_{1-x}Ca_xMnO_3$ ($0 \leq x \leq 0.5$) nanoparticles with nearly the same average grain size of about 21 nm and different Ca contents, $La_{0.8}Ca_{0.2}MnO_3$ nanoparticles with various average grain sizes were prepared. Crystal structure was investigated by X-ray diffraction. Increasing Ca content and decreasing grain size can lead to the average Mn–O bond lengths decrease and Mn–O–Mn bond angles increase. The crystal symmetry changes from orthorhombic to cubic as $x \geq 0.3$ for the $La_{1-x}Ca_xMnO_3$ ($0 \leq x \leq 0.5$) nanoparticles with nearly the same average grain size and $D \sim 16$ nm for the $La_{0.8}Ca_{0.2}MnO_3$ nanoparticles with various grain sizes. Small-size effect and surface effect may be the reasons of the lattice distortion and structure transition.

Keywords: Complex manganites; nanoparticles; crystal structure.

1. Introduction

Perovskites $A_{1-x}A'_xMnO_3$ (A = rare-earth, A' = alkaline-earth) compounds have been systematically investigated for single crystals, thin films and polycrystalline samples, due to their importance for fundamental research and potential applications.[1–3] For example, the structure and physical properties of this kind of compounds have been studied by changing temperature, applied pressure, doping level (x) and A-site average ionic radius ($\langle r_A \rangle$).[4–7] Recently, attention has been drawn towards nanocrystalline perovskite manganites. Mahesh *et al.*[8] investigated the effects of particle size on the electron transport and magnetic properties of $La_{0.7}Ca_{0.3}MnO_3$ and found that the T_c and metal-insulator transition temperature decrease with the particle size decreases. Surface spin-glass behavior has been observed in $La_{0.67}Sr_{0.33}MnO_3$ nanoparticles.[9] However, these researches are not enough, more detailed investigation is still required. In this report, we synthesize $La_{1-x}Ca_xMnO_3$ ($0 \leq x \leq 0.5$) nanoparticles and study its crystal structure. The dependence of the crystal structure on grain sizes and Ca contents for the $La_{1-x}Ca_xMnO_3$ nanoparticles will also be discussed.

*Corresponding author.

2. Experimental Procedure

$La_{1-x}Ca_xMnO_3$ ($x = 0, 0.1, 0.2, 0.3, 0.5$) nanoparticles were prepared using sol-gel method. La_2O_3, $MnCO_3$, $CaCO_3$ and a dispersion agent were dissolved in dilute nitric acid to get transparent solutions. Evaporating the water in the solutions, the viscous gels were dried and then calcined at different temperatures to get the desired products.

Powder X-ray diffraction (XRD) data were collected using a rotating-target X-ray diffractometer (Rigaku D/Max-2400) equipped with a graphite monochromator. The average grain sizes were estimated according to Scherrer equation and the diffraction peak widths. In order to gain the structure information at room temperature, the crystal structure of the $La_{1-x}Ca_xMnO_3$ nanoparticles were refined by the Rietveld refinement. The X-ray powder diffraction datas were recorded at $20^\circ \sim 100^\circ$ with a step of 0.02° and a counting time of 3 s per step. The rietveld refinement was performed using the program DBWS-9807a.[10]

3. Results and Discussion

The X-ray powder diffraction patterns of the $La_{1-x}Ca_xMnO_3$ nanoparticles show that all the samples are single-phase. The broad diffraction peaks are indicative of the ultrafine particles prepared. Analysis of the full patterns and of individual reflections reveals that the $La_{1-x}Ca_xMnO_3$ nanoparticles are orthorhombic symmetry and the intensity of some small diffraction peaks belonging to the orthorhombic structure weakens gradually with Ca contents increase and grain sizes decrease. In spite of this, the information of the crystallographic structure of the $La_{1-x}Ca_xMnO_3$ nanoparticles were obtained using the *Pnma* space group and the Rietveld refinement. The top panel of Fig. 1 shows a typical example of a fitted diffraction pattern for the $La_{0.8}Ca_{0.2}MnO_3$ nanoparticles with average grain size of about 21 nm. An agreement between the observed and calculated patterns is very good. The calculated average Mn–O bond length and Mn–O–Mn bond angle in variation with the Ca content x and grain size D are shown in Figs. 2 and 3.

From Figs. 2 and 3, we can see the tendency of the structure parameters in variation with the Ca content x and grain size D. By increasing x, the average Mn–O bond length becomes shorter and Mn–O–Mn bond angle becomes larger. Due to the slight difference between the ionic radii of La^{3+} and Ca^{2+}, the substitution of Ca^{2+} for La^{3+} may decrease the average ionic size at the La^{3+}/Ca^{2+} site. The substitution of the Ca^{2+} ions also may lead to formation of Mn^{4+} and increase the covalence between the Mn and O ions. These two factors made the Mn–O bond length decrease. As the deviation of the Mn–O–Mn bond angles from the ideal value of 180° in the cubic perovskite is related with the tilting of the MnO_6 octahedra, the tilting angle ω of the MnO_6 octahedra can be defined as $\omega = (\pi - \theta)/2$, where θ is the Mn–O–Mn bond angle. Hence, increasing Ca contents can decrease deviation of the Mn–O–Mn bond angle from the ideal value of 180° and the tilting of the MnO_6 octahedra. For the $La_{0.8}Ca_{0.2}MnO_3$ nanoparticles with the various average

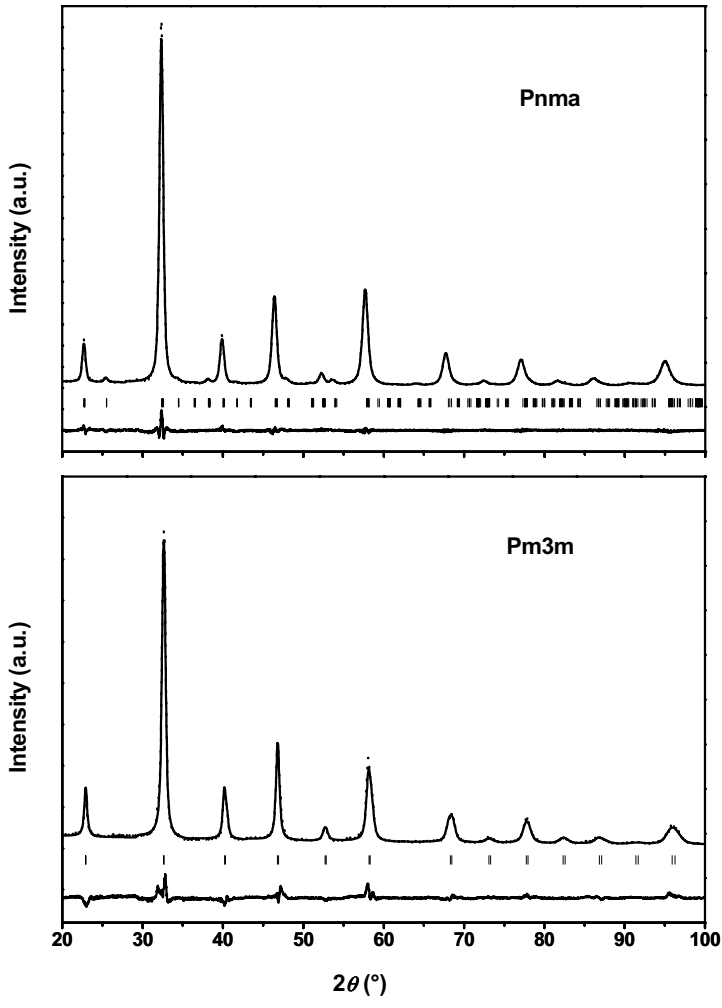

Fig. 1. Rietveld plots of X-ray diffraction patterns of the $La_{0.8}Ca_{0.2}MnO_3$ (top panel) and $La_{0.7}Ca_{0.3}MnO_3$ (bottom panel) nanoparticles with the average grain size of about 21 nm at 300 K. The solid line is the observed profile. The dot line is the calculated profile. The vertical marks below the profile show the position of allowed reflections. A difference curve (observed minus calculated) is plotted at the bottom.

grain sizes, a decrease of the average Mn–O bond length and an increase of the average Mn–O–Mn bond angle with decreasing grain sizes can be seen in Fig. 3. It indicates that decreasing grain sizes can decrease the lattice distortion and the tilting of the MnO_6 octahedra.

Analyzing the tilting angle ω, we find that $\omega \sim 0$ as $x \geq 0.3$ for the $La_{1-x}Ca_xMnO_3$ ($0 \leq x \leq 0.5$) and $D = 16$ nm for the $La_{0.8}Ca_{0.2}MnO_3$ nanoparticles, which is the character of cubic perovskite. In order to prove it clearly, we will study lattice constants of the $La_{1-x}Ca_xMnO_3$ nanoparticles.

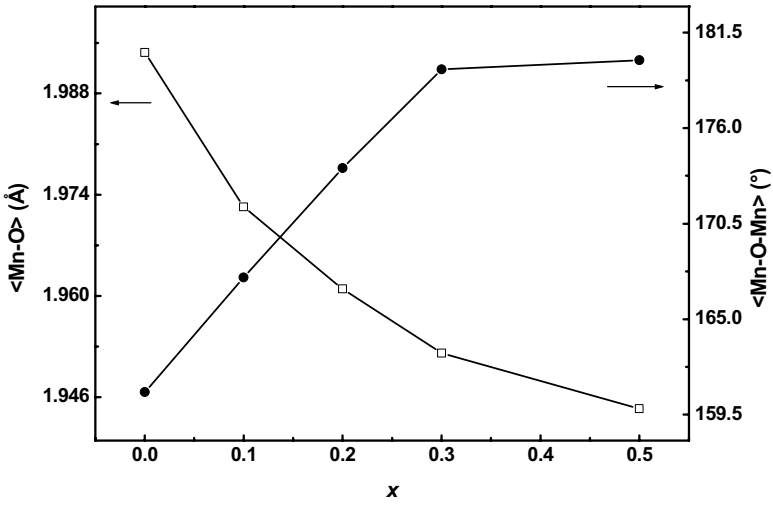

Fig. 2. Variations of the average Mn–O bond length and Mn–O–Mn bond angle versus Ca content x in $La_{1-x}Ca_xMnO_3$ $(0 \leq x \leq 0.5)$ nanoparticles.

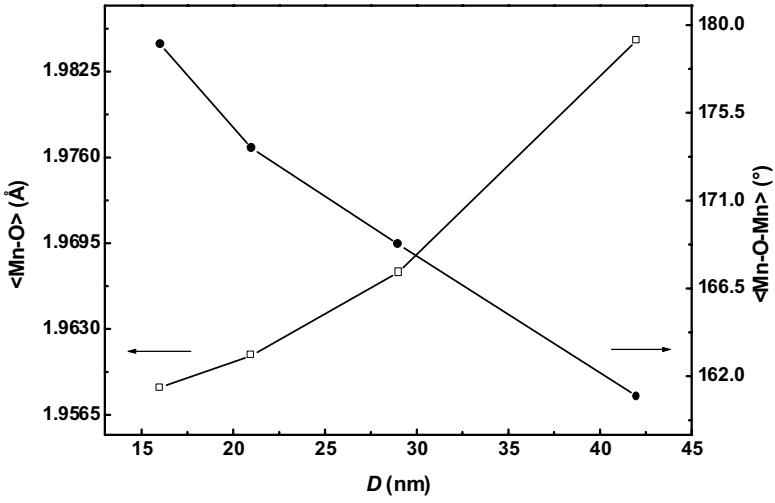

Fig. 3. Variations of the average Mn–O bond length and Mn–O–Mn bond angle versus the average grain size D in $La_{0.8}Ca_{0.2}MnO_3$ nanoparticles.

The lattice constants as a function of the Ca content x for the $La_{1-x}Ca_xMnO_3$ nanoparticles and of the grain size D for the $La_{0.8}Ca_{0.2}MnO_3$ nanoparticles are shown in Figs. 4 and 5. From Figs. 4 and 5, we see that a, b and c decrease linearly with increasing Ca content x and grain size D, and satisfy the relationship $a = c = b/\sqrt{2}$ as $x \geq 0.3$ for the $La_{1-x}Ca_xMnO_3$ $(0 \leq x \leq 0.5)$ and $D = 16$ nm for the $La_{0.8}Ca_{0.2}MnO_3$ nanoparticles, which is the character of cubic symmetry. So we refined the crystal structure of the $La_{1-x}Ca_xMnO_3$ $(0.3 \leq x \leq 0.5)$ and

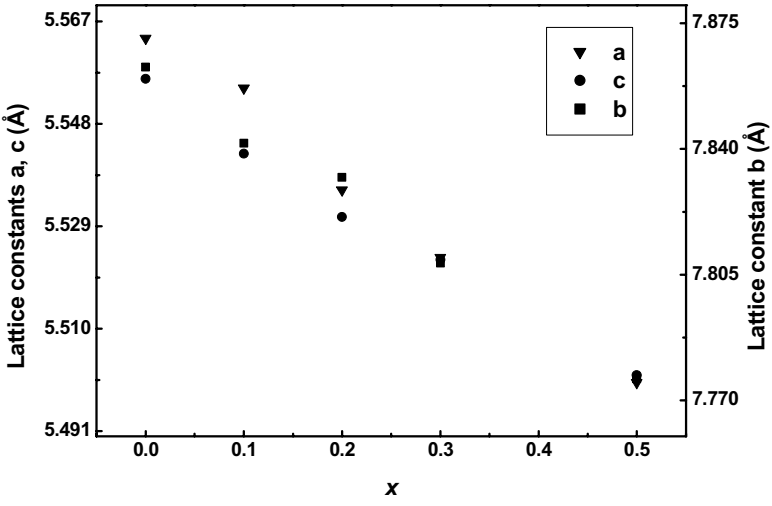

Fig. 4. Variations of the lattice constants a, b and c versus Ca content x in $La_{1-x}Ca_xMnO_3$ $(0 \leq x \leq 0.5)$ nanoparticles.

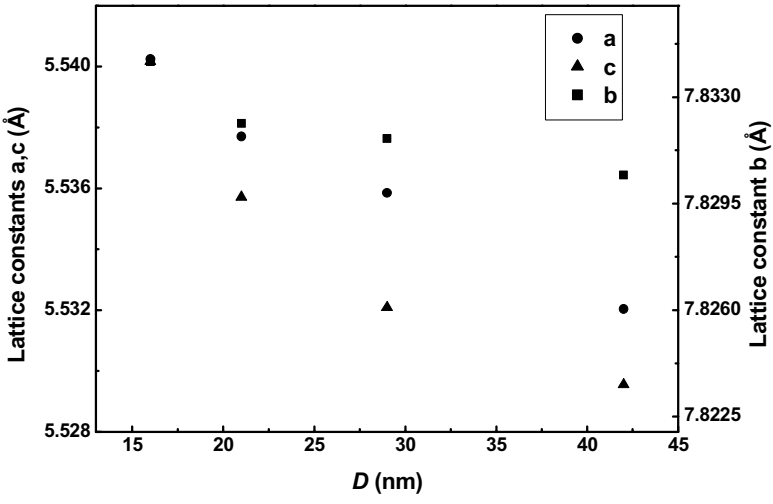

Fig. 5. Variations of the lattice constants a, b and c versus the average grain size D in $La_{0.8}Ca_{0.2}MnO_3$ nanoparticles.

$La_{0.8}Ca_{0.2}MnO_3$ ($D = 16$ nm) nanoparticles using the $Pm3m$ space group and the Rietveld refinement. The bottom panel of Fig. 1 shows a typical example of a fitted diffraction pattern for the $La_{0.7}Ca_{0.3}MnO_3$ nanoparticles with the average grain size of about 21 nm.

The coarse-grained $La_{1-x}Ca_xMnO_3$ $(0 \leq x \leq 0.5)$ polycrystals are orthorhombic structure,[11] but their nanoparticles have two phase structures. Perhaps internal pressure produced by surface stress and small grain diameter can explain it,

namely,[12] $\Delta p = 4\sigma_s/D$, where Δp is the difference between external and internal pressure, σ_s is the surface stress and D is the grain diameter. If surface stress of a grain size $D \sim 20$ nm is 10 N/m, the corresponding internal pressure is about 2 GPa, this value is rather large and can cause phase transition just like applied pressure.[13]

From Fig. 5, we also see that decreasing grain size can cause cell volume expansion, this can be explained by surface effect of the nanoscale particles, i.e. with decreasing particle sizes, the number of surface atoms increases, the atomic disorder and reduced coordination of the surface atoms can cause the lattice distortion of the surface atoms.

4. Conclusion

The $La_{1-x}Ca_xMnO_3$ ($0 \leq x \leq 0.5$) nanoparticles with nearly the same average grain size and different Ca contents, and the $La_{0.8}Ca_{0.2}MnO_3$ nanoparticles with various average grain sizes have structure transition at $x \sim 0.3$ and $D \sim 16$ nm, respectively. Increasing Ca content x and decreasing grain size D can decrease the average Mn–O bond length and the tilting of the MnO_6 octahedra.

References

1. R. Wang, R. Mahesh and M. Itoh, *Phys. Rev.* **B60** (1999) 14513–14516.
2. Y. Tomioka, A. Asamitsu and Y. Tokura, *Phys. Rev.* **B63** (2000) 24421–24426.
3. Z. H. Wang, G. Cristiani and H. U. Habermeier, *Appl. Phys. Lett.* **82** (2003) 3731–3733.
4. B. Dabrowski, X. Xiong, Z. Bukowski, R. Dybzinski, P. E. Klamut, J. E. Siewenie, O. Chmaissem, J. Shaffer and C. W. Kimball, *Phys. Rev.* **B60** (1999) 7006–7017.
5. H. Y. Hwang, S.-W. Cheong, P. G. Radaelli, M. Marezio and B. Batlogg, *Phys. Rev. Lett.* **75** (1995) 914–917.
6. P. G. Radaelli, G. Iannone, M. Marezio, H. Y. Hwang, S.-W. Cheong, J. D. Jorgensen and D. N. Argyriou, *Phys. Rev.* **B56** (1997) 8265–8276.
7. Y. Moritomo, A. Asamitsu and Y. Tokura, *Phys. Rev.* **B51** (1995) 16491–16494.
8. R. Mahesh, R. Mahendiran, A. K. Raychaudhuri and C. N. R. Rao, *Appl. Phys. Lett.* **68** (1996) 2291–2293.
9. T. Zhu, B. G. Shen, J. R. Sun, H. W. Zhao and W. S. Zhan, *Appl. Phys. Lett.* **78** (2001) 3863–3865.
10. R. A. Young, A. C. Larson and C. O. Paiva-Santos, *Program DBWS-9807a for Rietveld Analysis of X-ray and Neutron Powder Diffraction Patterns* (Atlanta, 1999).
11. P. G. Radaelli, D. E. Cox, M. Marezio and S.-W. Cheong, *Phys. Rev.* **B55** (1997) 3015–3023.
12. M. Winterer, R. Nitsche, S. A. T. Redfern, W. W. Schmahl and H. Hahn, *Nanostruct. Mater.* **6** (1995) 679–688.
13. T. Wu, K. Fossheim and T. Lægreid, *Solid State Commun.* **80** (1991) 47–50.